

Article

# A Data-Driven Method for Ship Motion Forecast

Zhiqiang Jiang, Yongyan Ma and Weijia Li \*

School of Naval Architecture and Ocean Engineering, Huazhong University of Science and Technology, 1037 Luoyu Road, Hongshan District, Wuhan 430074, China

\* Correspondence: liweijia@hust.edu.cn; Tel.: +86-13507114896

**Abstract:** Accurate forecasting of ship motion is of great significance for ensuring maritime operational safety and working efficiency. A data-driven ship motion forecast method is proposed in this paper, aiming at the problems of low generalization of a single forecast model and insufficient forecast accuracy under unknown conditions. First, the fluid dynamics simulations of the ship are carried out under multiple node conditions based on overset mesh technology, and the obtained motion data is used for training the Bidirectional Long Short-term Memory network models. One or more pre-trained forecast models would be selected based on the correlation of condition nodes when forecasting ship motion under non-node conditions. The Golden Jackal Optimization Algorithm is used to compute the regression coefficient of each node model in real time, and finally, the dynamic model average is calculated. The results show that the method proposed in this study can accurately forecast the pitch and heave of the KCS ship in 5 s, 10 s, and 15 s of forecast duration. The accuracy of the multi-order forecast model improves more in longer forecast duration tasks compared with the first-order model. When forecasting ship motion under non-node conditions, the method shows stronger model generalization capabilities.

**Keywords:** ship motion forecast; CFD; BiLSTM; Golden Jackal Optimization



**Citation:** Jiang, Z.; Ma, Y.; Li, W. A Data-Driven Method for Ship Motion Forecast. *J. Mar. Sci. Eng.* **2024**, *12*, 291. <https://doi.org/10.3390/jmse12020291>

Academic Editors: Nastia Degiuli and Ivana Martić

Received: 11 January 2024

Revised: 2 February 2024

Accepted: 3 February 2024

Published: 5 February 2024



**Copyright:** © 2024 by the authors. Licensee MDPI, Basel, Switzerland. This article is an open access article distributed under the terms and conditions of the Creative Commons Attribution (CC BY) license (<https://creativecommons.org/licenses/by/4.0/>).

## 1. Introduction

In the course of offshore operations in real maritime environments, ships are affected by environmental factors such as wind, waves, and currents, resulting in motion with six degrees of freedom. Abrupt changes in ship motion have the potential to inflict damage upon equipment, interrupt work processes, or cause harm to personnel [1]. By forecasting ship motion, measures can be taken in advance to ensure the stability of equipment, thereby enhancing the safety of offshore operations. Simultaneously, high-precision compensation for ship motion reduces the impact of waves and currents on the ship, enabling engineering equipment to operate more stably. In engineering operations necessitating precision, such as offshore lifting and ship replenishment, the stability of equipment proves crucial for the execution of operations [2]. Accurate forecasting of ship pitch and heave holds significant importance for the maritime operations of engineering ships, contributing to enhanced safety in offshore operations and the reduction of maritime incidents [3]. As a result, research on ship motion forecasting has consistently garnered significant attention.

Currently, time series forecasts are predominantly categorized into two groups: those based on mathematical model methods and those utilizing machine learning techniques [4]. Mathematical model methods for forecasts encompass approaches such as the Kalman Filter, Autoregressive Integrated Moving Average model, and others. Nie, ZH et al. introduced a detrended autoregressive (AR) model based on detrended fluctuation analysis (DFA) for forecasting the motion of large ships [5]. Peng, XY et al. proposed an improved unscented Kalman filter (MUKF) algorithm proficient in mitigating the impact of abnormal data on dynamic positioning ship motion state estimation [6]. Jiang, H, et al. investigated hull scale effects in real-time motion using an autoregressive (AR) model, revealing a negative correlation between prediction accuracy, and spectrum bandwidth, and peak

frequency [7]. Takami, T et al. utilized the autocorrelation function (ACF) of short-term measurements for real-time deterministic forecasting of ship motion induced by waves [8]. Mathematical model-based forecasting methods typically exhibit high complexity and low computational efficiency. Furthermore, the capacity of such mathematical models to forecast non-stationary nonlinear time series is somewhat restricted, such as ship motion in irregular waves.

Neural network models demonstrate the ability to learn and capture intricate, nonlinear relationships. In the case of time series data involving multiple variables and interaction effects, neural networks can perform learning without the need for explicit data preprocessing, showing flexibility in forecasting tasks for nonlinear time series [9]. D'Agostino, D et al. conducted performance tests on Recurrent Neural Networks (RNN), Long Short-term Memory Neural Networks (LSTM), and Gate Recurrent Unit models (GRU) using computational fluid dynamics data from self-propelled destroyer-type ships [10]. Silva, K.M et al. utilized motion data from the DTMB5415 ship model in long-peak irregular waves to establish a ship motion prediction system based on LSTM, aiming to predict the ship motion response induced by waves [11]. Diez, M et al. proposed an equation-free ship motion response prediction method based on dynamic mode decomposition (DMD) and analyzed the navigation data of the free-sailing DTMB5415 ship and the KRISO ship [12].

Even though neural network models excel at handling complex nonlinear relationships and offer numerous advantages in time series forecasting, deep neural networks are often considered black-box models, with the internal representations being challenging to interpret [13]. The lack of interpretability can be a limitation in certain applications where a clear understanding of the model is essential. Consequently, some studies have emerged that seek to combine the strengths of mathematical models and neural networks to achieve comprehensive ship motion forecasts. Suhermi, N et al. combined an autoregressive integral moving average model with an artificial neural network (ANN) to predict the rolling motion of a floating production unit (FPU). The findings indicated that the ARIMA model was more adept at capturing the linear characteristics of motion, while the ANN model exhibited superior fitting characteristics for the nonlinear aspects of the model [14]. Xu, WZ et al. utilized second-order wave theory data to employ the LSTM model in predicting the intricate nonlinear input-output relationships within ocean systems [15]. Additionally, some researchers have explored using pre-trained neural network models for predicting new data through transfer learning. Ye R et al. proposed a hybrid algorithm (TrEnOS-ELMK) based on transfer learning an online sequential extreme learning machine with a kernel (OS-ELMK), and ensemble learning. This approach effectively leverages latent knowledge from past data to make predictions about future data [16]. YT Du et al. proposed AdaRNN for transfer learning on time series regression and prediction tasks, addressing the Temporal Covariance Shift (TCS) problem [17]. Transfer learning has demonstrated excellent performance in human activity identification, air quality prediction, and financial analysis. However, the continuous data distribution in time series poses challenges, leading to the instability of data distribution. Additionally, the intricate structure and gradient propagation issues of RNN complicate the direct application of existing transfer learning methods. These challenges may hinder the effective transfer of pre-trained forecast models to the task of ship motion forecasting in unknown conditions.

In time series forecasting, the predictive performance of a single model is often constrained by its structure and parameter selection, leading to limitations such as the absence of estimates for uncertainty in model outputs. While a model may perform well on training data, it may underperform in generalizing effectively to new series. Model averaging is a technique that addresses these challenges by combining predictions from multiple models [18]. When faced with changing data distributions or uncertainties, model averaging proves valuable in mitigating the risk of overfitting that a single model may encounter under specific conditions, thereby enhancing the robustness of the forecasting model. Darbandsari, P et al. proposed an entropy-based Bayesian model averaging (BMA) algorithm, utilizing it in daily flow prediction across various watersheds [19]. Naser, H used dy-

dynamic model averaging (DMA) to forecast West Texas Intermediate crude oil (WTI) prices. The results demonstrated that the dynamic model averaging method outperformed other alternative models used in the forecasting exercise [20].

Most existing forecast methods for ship motion rely on given ship motion data, utilizing either mathematical models or machine learning techniques to create a priori ship motion response forecasting models. However, these models often lack generalization ability under new conditions, leading to a decrease in prediction performance when confronted with changing ship operation conditions. In ship motion forecasting, the characteristics and distributions of ship motion time series vary under different conditions. The actual conditions often differ from those encountered during pre-training, leading to the inability of the pre-trained model to accurately forecast new conditions. Due to disparities in the spatiotemporal characteristics between datasets, the model may overly adapt to the spatiotemporal features of specific conditions, resulting in a diminished ability to generalize to other conditions. A data-driven ship motion forecasting method is proposed in this paper to address this challenge, building on the research conducted by previous researchers [10,20–23]. The approach employs one or more pre-trained neural network models to forecast ship motion under unknown conditions. Initially, numerous numerical simulations are conducted on the target ship in various sea states or wave approach angles, utilizing overset grid technology. The motion and wave elevation data are then used to train Bidirectional Long Short-term Memory network models (BiLSTM). When forecasting pitch and heave under unknown conditions, multiple pre-trained node models are selected. The Golden Jackal Optimization Algorithm (GJO) is employed to compute the regression coefficients for each pre-trained node model, and the Dynamic Model Averaging (DMA) is calculated. The diversity of sea conditions and ship motion states are taken into account in the method, resulting in more comprehensive and reliable forecasts. The model becomes better adapted to the complexities of ship motion in diverse sea states by leveraging data from each node’s conditions. This approach (see Figure 1) holds significant importance for enhancing offshore operation safety and improving operational efficiency.

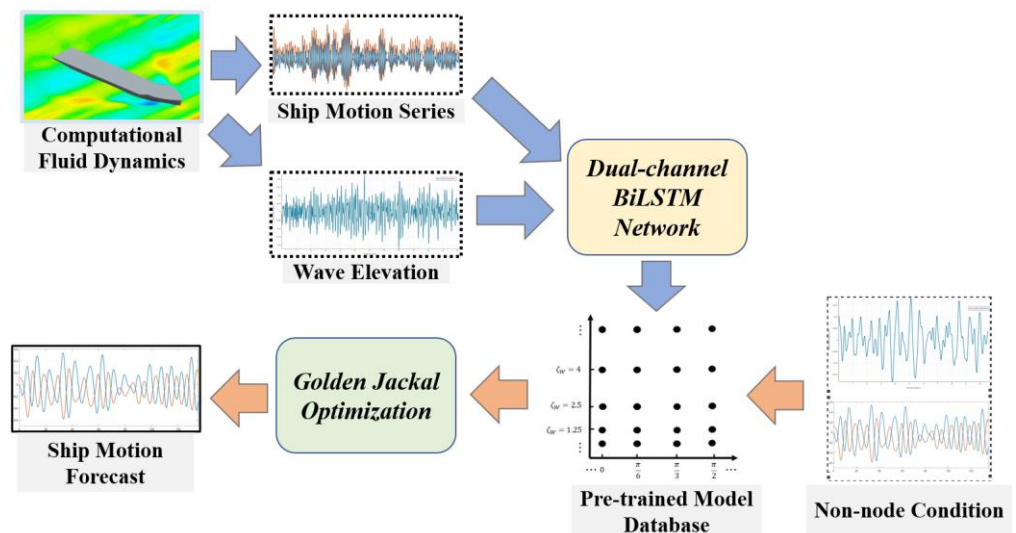


Figure 1. Model Framework.

## 2. Methods

### 2.1. Ship Motion Response Model

The irregular motion of a ship is induced by the influence of irregular waves. When ships perform offshore operations in relatively stable sea conditions, it can be assumed to function as a time-invariant linear system [24]. In this research, the disturbance is

represented by the wave passing through the hull. The ship's 6-dof motion serve as the system's responses. The system input and output can be described as:

$$Y(t) = L[\zeta(t)] \tag{1}$$

where,  $\zeta(t)$  represents the time series of wave elevation and  $Y(t)$  is the ship's motion response. When the wave elevation input consists of regular sinusoidal waves, the dynamic characteristics of the ship can be described using a frequency response function within the frequency domain. The relationship between the dynamic input  $\zeta(t)$  and output  $Y(t)$  of a linear system can be expressed using constant-coefficient differential equations:

$$\sum_{i=0}^n b_{n-i} \frac{d^{n-i} Y}{dt^{n-i}} = \sum_{j=0}^m a_{m-j} \frac{d^{m-j} \zeta}{dt^{m-j}} \tag{2}$$

The equation above is Laplace transformed and let  $S = j\omega$ , the transfer function of the linear system can be derived as:

$$Y_{y\zeta}(j\omega) = \frac{Y(j\omega)}{\zeta(j\omega)} = \frac{Y_0}{\zeta_0} e^{j\delta} \tag{3}$$

where,  $Y_0/\zeta_0$  represents the amplitude-frequency characteristics of the system and  $e^{j\delta}$  denotes the phase-frequency characteristics of the system.  $Y_{y\zeta}$  is the 6-dof motion response function of the ship. In real maritime conditions, wind and waves are highly irregular, with the amplitude, wavelength, and period of each wave being subject to random variations. According to the principle of linear superposition of irregular waves, the energy of irregular waves is equal to the sum of the energies of individual regular waves [25]. The distribution of energy across different frequency components of irregular waves can be described using the wave spectrum density function:

$$S_{\zeta}(\omega) = \frac{\zeta_a^2}{2\Delta\omega} \tag{4}$$

where,  $S_{\zeta}(\omega)$  represents the wave spectrum density function and  $\zeta_a$  is the wave amplitude. Therefore, when the wave elevation input is an irregular wave, the ship's motion at any given moment can be considered the superposition of the motion generated under the input of individual regular waves, expressed as:

$$Y(t) = \sum_{n=1}^{\infty} Y_{y\zeta}(\omega_n) \zeta_{an} \cos(K_n \zeta - \omega_n t + \varepsilon_n) \tag{5}$$

where,  $\zeta_{an}$  is the amplitude of individual regular waves,  $K_n$  is the wave number of individual regular waves,  $\omega_n$  is the circular frequency of individual regular waves, and  $\varepsilon_n$  is the phase of individual regular waves. According to the energy superposition theorem and referencing the wave spectrum density function, the motion spectrum density function of the ship under irregular waves is defined as:

$$S_{y\zeta}(\omega) = \frac{[Y_{y\zeta}(\omega) \zeta_a]^2}{2\Delta\omega} = Y_{y\zeta}^2(\omega) \cdot S_{\zeta}(\omega) \tag{6}$$

where,  $Y_{y\zeta}^2$  represents the system response amplitude operator. It can be seen from the equation that the motion response of the ship is simultaneously influenced by both the ship's intrinsic factors and environmental factors. In this study, the Pierson-Moskowitz wave spectrum is used for the numerical simulation of irregular waves. The P-M spectrum

is a semi-empirical wave spectrum, primarily derived from well-developed waves in the Atlantic [26].

$$S_{\zeta}(\omega) = \frac{0.78}{\omega^5} \exp\left(-\frac{0.74g^4}{U^4\omega^4}\right) \tag{7}$$

where,  $U$  is the average wind speed at a height of 19.5 m, and the approximate relationship with the significant wave height is given by  $U = 6.85\sqrt{\bar{\zeta}_W}$ . Consequently, the relationship between the Pierson-Moskowitz spectrum and the significant wave height can be obtained as:

$$S_{\zeta}(\omega) = \frac{0.78}{\omega^5} \exp\left(-\frac{1}{\bar{\zeta}_W^2} \cdot \frac{0.74g^4}{6.85^4\omega^4}\right) \tag{8}$$

While a ship is moored at sea for offshore operation, the navigational speed  $V = 0$ , and the encounter frequency  $\omega_e$  of the waves are the same as the original wave frequency  $\omega$ . When there is a wave approach angle  $\mu$  between the wave propagation direction and the ship's heading, the wavelength  $\lambda_1$  through the ship's longitudinal section is given by:

$$\lambda_1 = \frac{\lambda}{\cos\mu} \tag{9}$$

The simultaneous equations of the ship's pitch and heave motion response can be expressed as:

$$\begin{pmatrix} S_{\psi\zeta} \\ S_{Z\zeta} \end{pmatrix} = \begin{cases} F_{\psi,Z}(\mu, \bar{\zeta}_W^2) \\ M_{\psi,Z}(\mu, \bar{\zeta}_W^2) \end{cases} \tag{10}$$

From the equations above, it is evident that the ship's motion response equation can be treated as an implicit function of the wave approach angles  $\mu$  and the significant wave height  $\bar{\zeta}_W$ . The time series of ship motions under each condition node are used for training neural network models, thereby obtaining the respective motion forecasting models. Due to the fact that ships cannot be treated as a linear system under rough sea conditions, this research predominantly focuses on the prediction of pitch and heave of ships under the upper limit of level-6 sea state.

### 2.2. BiLSTM Network

Bidirectional Long Short-Term Memory (BiLSTM) is a variation of Recurrent Neural Network (RNN) designed for series processing. BiLSTM incorporates hidden layers in two directions: one for processing the sequence in chronological order (from past to future) and the other for processing the sequence in reverse order (from future to past) [27]. This framework is capable of considering both past and future contextual information, enhancing its ability to capture long-term dependencies within the sequence. The bidirectional information flow structure of BiLSTM enables the model to comprehensively capture the temporal dependencies in series, a crucial aspect for longer time series prediction tasks. Simultaneously, the bidirectional architecture helps alleviate issues related to gradients vanishing or exploding, contributing to a more stable training process. This is attributed to the fact that gradients can propagate from both directions, facilitating a smoother update of model parameters. For each time step, BiLSTM receives an input and produces an output. In sequence tasks, the output can be obtained at the last time step or at every time step, depending on the inherent nature of the task. The structure of a single-layer BiLSTM is illustrated in Figure 2:

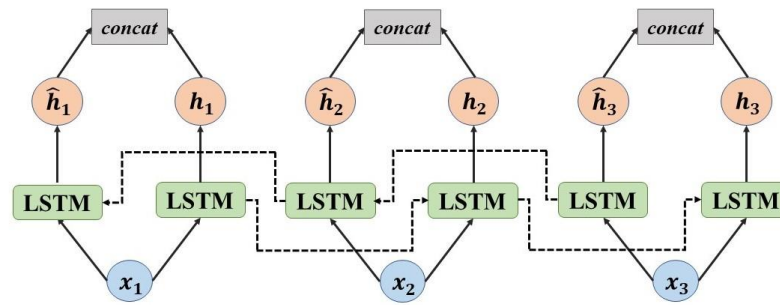


Figure 2. BiLSTM Network.

In contrast to the Gated Recurrent Unit (GRU) model, the BiLSTM model effectively addresses long-term dependencies through the incorporation of explicit memory units. Despite the relatively intricate structure and parameter abundance inherent, BiLSTM consistently demonstrates superior performance in the context of intricate sequential tasks, particularly those demanding the retention of long-term memory. Long Short-Term Memory (LSTM) is a type of recurrent neural network designed for processing sequential data [28]. LSTM manages the information flow through gating units, including input gates, forget gates, and output gates, enabling effective handling of long-term dependencies. Bidirectional LSTM (BiLSTM) enhances the network’s capability to model long-term dependencies by employing LSTM units in both forward and reverse directions. In this study, the Dual-channel BiLSTM network (see Figure 3) is employed to train ship motion forecasting models under various node conditions, with forecast durations of 5 s, 10 s, and 15 s. Subsequently, the method generates pre-trained forecast models corresponding to each node condition and makes forecasts for ship motion under non-node conditions.

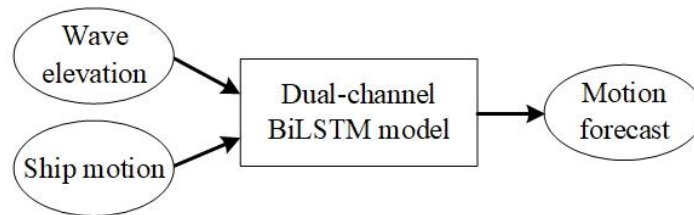


Figure 3. Dual-channel Forecasting Model.

### 2.3. Dynamic Model Averaging Based on GJO

The ship’s motion response varies significantly under different conditions, especially with varying wave approach angles and sea states. A single pre-trained model struggles to provide accurate predictions for ship motion. Therefore, an effective method is essential for accurately forecasting the ship’s motion in various conditions. This study employs a dynamic model averaging based on the Golden Jackal algorithm to forecast ship motion responses. The main method is to leverage pre-trained ship motion forecast models under multiple node conditions to forecast the ship’s motion under non-node conditions. By systematically modeling the ship’s motion response under different node conditions, the motion characteristics in diverse environments can be captured. These condition nodes correspond to different sea states and navigational speeds, forming a multidimensional parameter space for the model database. The Golden Jackal algorithm is utilized to calculate the dynamic regression coefficients for multiple node condition models under unknown conditions, facilitating the forecast of ship motion responses.

Dynamic Model Averaging (DMA) is a model ensemble method employed to amalgamate predictions from multiple models, thereby enhancing overall performance. In contrast to conventional model averaging approaches, dynamic model averaging enables the adaptive adjustment of model weights over time to accommodate alterations in data

distribution or shifts in model performance [29]. The state space model of dynamic model averaging encompasses the following components:

$$y_t = x_t^T \alpha_t + \varepsilon_t \tag{11}$$

$$\alpha_t = \alpha_{t-1} + \delta_t \tag{12}$$

where,  $y_t$  is the deviation of the output thickness of samples,  $x_t^T$  is the corresponding vector of independent variables of the regression model,  $\alpha_t$  is a vector of regression parameters, and the innovations  $\varepsilon_t, \delta_t$  are distributed in a Normal distribution with a mean of 0. In real sea conditions, the significant wave height and wave approach angle of the ship often deviate from those of the condition nodes. When forecasting ship motion under such non-node conditions, a thorough assessment must be conducted, taking into account nearby node conditions. This method employs one or more comparable ship motion forecast models for predictions, followed by the result of the dynamic model average. The pseudocode of the condition node selection Algorithm 1 is as follows:

---

**Algorithm 1:** Condition Node Select

---

**Input:**  $[m, n]$ , where  $m$  and  $n$  are parameters of ship motion response functions; Condition nodes coordinate sets  $X, Y$

**Output:** Condition Nodes

- 1  $X(m+), Y(n+)$ : **Node greater than  $m$  or  $n$  in that dimension;**
  - 2  $X(m-), Y(n-)$ : **Node less than  $m$  or  $n$  in that dimension;**
  - 3 **if**  $m \in X$  **and**  $n \in Y$  **then**
  - 4     Condition Nodes  $\leftarrow \{[m, n]\}$ ;
  - 5 **else if**  $m \in X$  **and**  $n \notin Y$  **then**
  - 6     Condition Nodes  $\leftarrow \{[m, Y(n+)], [m, Y(n-)]\}$ ;
  - 7 **else if**  $n \in Y$  **and**  $m \notin X$  **then**
  - 8     Condition Nodes  $\leftarrow \{[X(m+), n], [X(m-), n]\}$ ;
  - 9 **else**
  - 10    Condition Nodes  $\leftarrow \{[X(m+), Y(n+)], [X(m+), Y(n-)], [X(m-), Y(n+)], [X(m-), Y(n-)]\}$ ;
  - 11 **return** Condition Nodes
- 

Algorithm 1 outputs one or more node operating conditions that are closest to the current condition. The pre-trained model is selected according to the node conditions output by Algorithm 1 in subsequent ship motion predictions. When forecasting ship motion under non-node conditions, the output of a single pre-trained node model can be expressed as:

$$Y(t) = \tilde{Y}(t) + \tilde{\varepsilon}(t) \tag{13}$$

where,  $Y(t)$  represents the actual ship motion response time series under the specific condition, while  $\tilde{Y}(t)$  denotes the motion time series predicted by the pre-training model. The term  $\tilde{\varepsilon}(t)$  corresponds to the forecast error. The relationship between the outcomes of multiple pre-training models and the actual motion series can be expressed as:

$$Y(t) = \sum_{i=1}^n \left[ \alpha_i \tilde{Y}_i(t) + \tilde{\varepsilon}_i(t) \right] = \sum_{i=1}^n \alpha_i \tilde{Y}_i(t) + \varepsilon(t) \tag{14}$$

where,  $\alpha_i$  represents the regression coefficients for each node forecast model, and  $n$  signifies the model order, indicating the count of participating pre-trained models in the forecast. The selection of the node model is determined by the correlation between the forecasting condition and the node conditions. To evaluate the correlation under a consistent standard

between the node conditions and the forecasting conditions, the significant wave heights and wave approach angles of the node conditions are subjected to Min–Max normalization. The normalization process ensures that the values remain characteristic features on the same scale. The formula for the model normalization calculation is:

$$x' = \frac{x - \min(x)}{\max(x) - \min(x)} \tag{15}$$

As the ship motion forecasts in this research are all conducted in relatively stable sea states, the significant wave height range aligns with the upper limit of sea states from level 0 to level 6. Additionally, the wave approach angles fall within the range  $[0, \pi/2]$ . For pitch and heave motions, the correlation coefficient  $R_{Z\psi}$  for the condition node is defined as:

$$R_{Z\psi} = \sqrt{(\mu - \mu_n)^2 + (\zeta - \bar{\zeta}_n)^2} \tag{16}$$

where,  $\mu_n$  and  $\bar{\zeta}_n$  represent the wave approach angle and significant wave height, respectively, under normalized node conditions. The selection of the node forecast model is based on the model correlation coefficient. When the model order  $n = 1$ , ship motion is forecasted solely by the pre-trained model of the node condition with the highest correlation. During this scenario, each ship motion forecast opts for the pre-trained model with the highest posterior probability, known as the Dynamic Model Selection (DMS) forecast. The selection of 1st to 4th-order forecast models is illustrated in Figure 4. For ship motion forecasts involving second-order models and beyond, this research employs the Golden Jackal optimization algorithm. The optimization process utilizes the absolute mean error as the objective function to determine and optimize the regression coefficients of each pre-trained model.

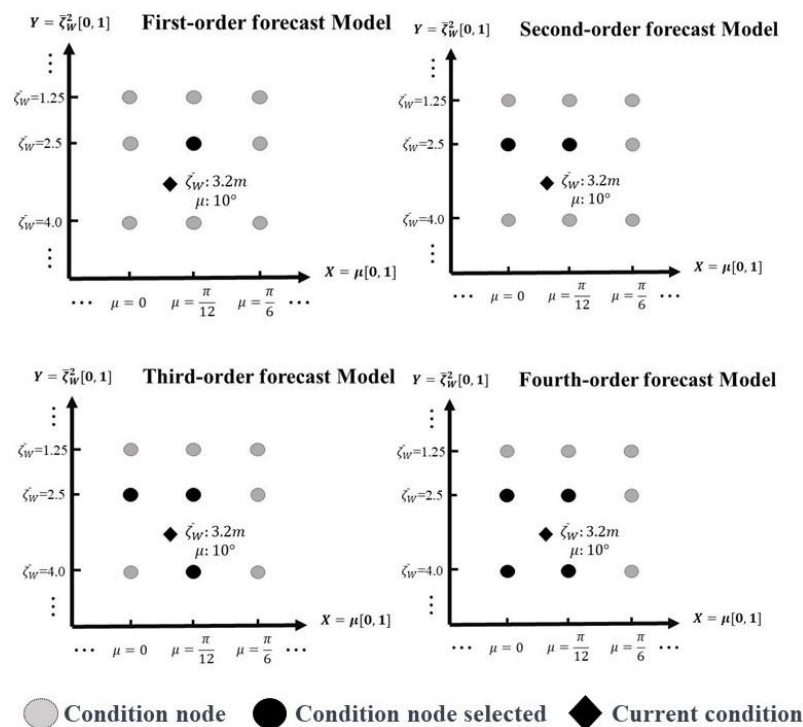


Figure 4. 1st–4th order Forecasting Model.

The Golden Jackal Optimization (GJO) is a global optimization algorithm inspired by the cooperative hunting behavior of golden jackals [30]. The GJO algorithm computes the fitness matrix using the prey population position matrix and a designated fitness function.

In the prey search stage, the mathematical model for the relative position of each individual in the prey population, inspired by the golden jackal, is expressed as follows:

$$\begin{cases} Y_{1i}(t) = Y_M(t) - E \cdot |Y_M(t) - rl \cdot X_i(t)| \\ Y_{2i}(t) = Y_{FM}(t) - E \cdot |Y_{FM}(t) - rl \cdot X_i(t)| \end{cases} \quad (17)$$

where,  $t$  denotes the current iteration count,  $X_i$  represents the position of the  $i$ -th prey,  $Y_M$  and  $Y_{FM}$  respectively indicates the positions of male and female golden jackals,  $rl$  signifies a random number based on the Levy distribution, and  $E$  denotes the prey's escape energy, calculated as follows:

$$rl = 0.05 \cdot LF() \quad (18)$$

$$E = 3(\text{random}[0,1] - 1) \cdot \left(1 - \frac{t}{T}\right) \quad (19)$$

where,  $LF()$  is the Levy flight function and  $T$  is the total number of iterations. During hunting, the relative position of the golden jackal is as follows:

$$\begin{cases} Y_{1i}(t) = Y_M(t) - E \cdot |rl \cdot Y_M(t) - X_i(t)| \\ Y_{2i}(t) = Y_{FM}(t) - E \cdot |rl \cdot Y_{FM}(t) - X_i(t)| \end{cases} \quad (20)$$

The regression coefficients of each pre-trained model are determined by the GJO algorithm according to the errors between real motion and predicted motion from the previous period. These regression coefficients are then utilized for forecasting the ship's motion in the subsequent time period. To maintain the model's timeliness, the regression coefficients for each pre-trained model are regularly recalculated at certain intervals.

### 3. Experiment

#### 3.1. Numerical Simulation of the KCS Ship

To validate the research methodology, a KCS ship model is employed as the subject for ship motion forecasting. As a standard ship model, the KCS model finds extensive application in towing tank experiments and numerical simulations. Figure 5 and Table 1 illustrate the KCS ship model along with its main parameters:



**Figure 5.** The KCS Hull Form.

**Table 1.** Main Geometric Parameters.

	Full Scale	Model
Scale	1	80.87
Length between perpendiculars (m)	230	2.844
Design waterline breadth (m)	32.2	0.398
Draught (m)	10.8	0.134
Displacement space(m <sup>3</sup> )	52,030	0.09836

The entire KCS ship model is used for numerical simulation under specific node conditions, leading to the establishment of the motion forecast model database. Node coordinates within the model database are defined based on a wave approach angle of 15° and a significant wave height from the sea state level (see Table 2) specified by the National Marine Environmental Forecasting Center of China [31]. The total number of condition

nodes is not fixed. The range and density of condition nodes are determined based on specific usage requirements. A broader range and higher density of nodes imply a more extensive and accurate forecast capability. However, it also results in a larger computational workload for simulations. In subsequent calculations, it is assumed that a full-scale ship is engaged in seaborne operations at a standstill while the waves move in relation to the ship at a speed of 7.71 m/s (15 kn). Adhering to the Froude similarity criterion and applying a scale ratio of 80.87, the length of the ship model is set to  $L = 2.844$  m, and the wave propagation speed is set to  $V = 0.858$  m/s. The motion series obtained from the simulation were enlarged in equal proportions according to the scale ratio of 80.87 and the Froude similarity criterion and used as the motion data of the full-scale ship for subsequent research.

**Table 2.** Sea State Level.

Level	Sea State	Wave Height
0	Calm-Glassy	0 m
1	Calm-Rippled	0–0.1 m
2	Smooth-Wavelet	0.1–0.5 m
3	Slight	0.5–1.25 m
4	Moderate	1.25–2.5 m
5	Rough	2.5–4.0 m
6	Very Rough	4.0–6.0 m

The mesh of the ship model is shown in Figure 6. According to the ITTC specifications, the numerical tank velocity inlet is positioned a ship length from the bow, the pressure outlet is located three ship lengths from the stern, and the side boundaries are set at one ship length. The total length of the domain is five ship lengths, while the total width is two ship lengths. Overset mesh is applied to the body and the background, with localized refinement at the free surface and hull [32]. The total number of mesh cells is 6 million. For this numerical simulation of irregular waves, the Pierson-Moskowitz wave spectrum is employed, and a probe is set a half-ship length from the bow to monitor wave elevation. When ships are navigating or operating at sea, a wave approach angle larger than  $75^\circ$  is uncommon. Beams in the sea or waves close to a  $90^\circ$  approach angle can significantly impact the safety of the ship. In more severe sea conditions, ships would not be qualified for maritime operations. Therefore, numerical simulations of ship motion based on sea state levels and a  $15^\circ$  angle difference are conducted in subsequent experiments. Figures 7 and 8 display the free surface and wave elevation.

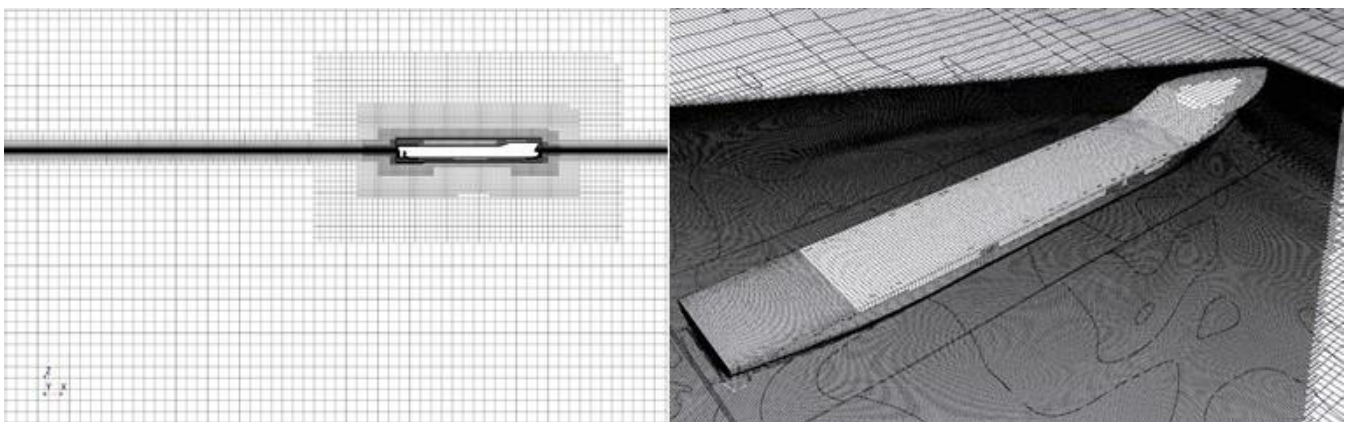


**Figure 6.** Computational Domain and Hull Mesh.

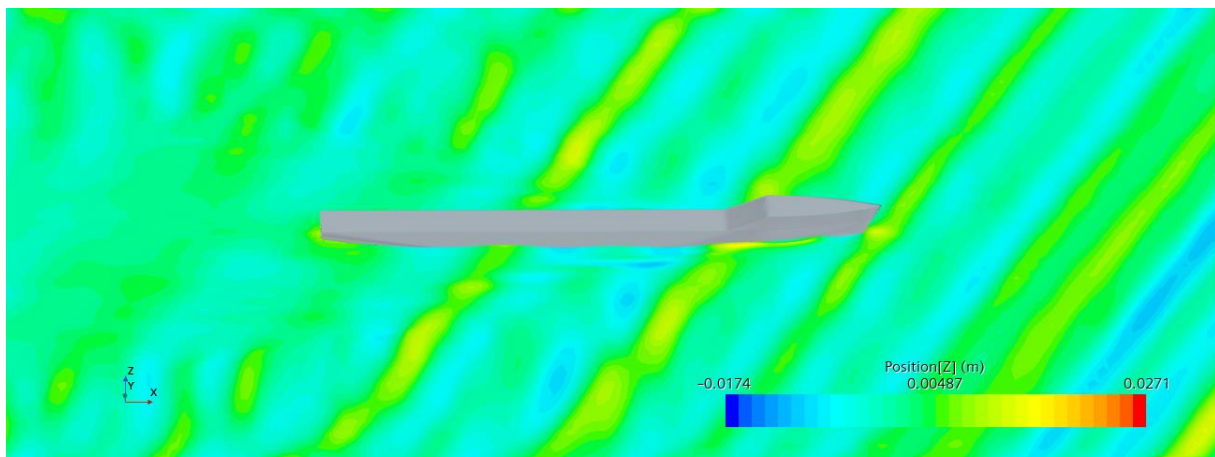


Figure 7. KCS Model on a Free Surface.

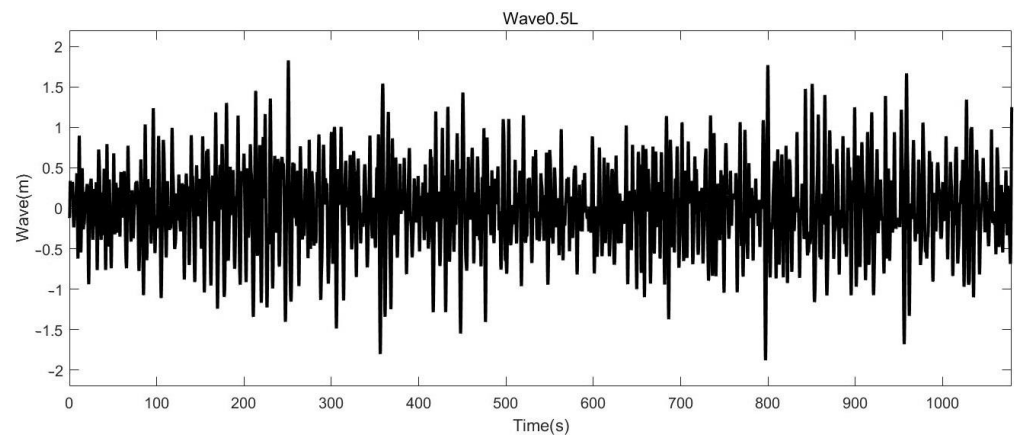


Figure 8. Wave Elevation at 0.5 L ( $\bar{z}_W = 2.5$  m).

In each numerical simulation, the time-domain response of the ship model’s pitch and heave motion under node conditions is sampled at a frequency of 100 Hz, serving as training data for the neural network model. The duration of the full-scale ship motion data for each condition is 1200 s. Part of the ship motion series is presented in Figures 9 and 10.

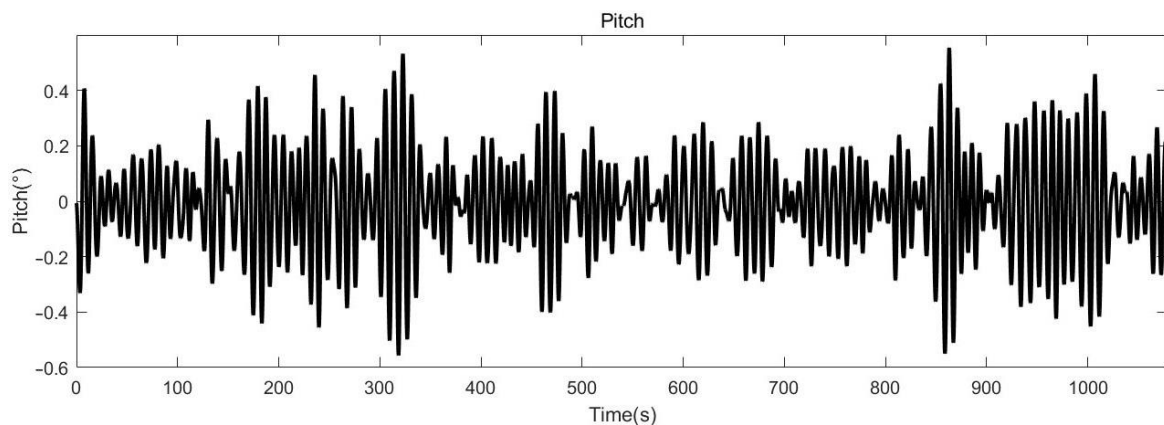


Figure 9. Pitch Time Series ( $\bar{z}_W = 2.5$  m,  $\mu = 15^\circ$ ).

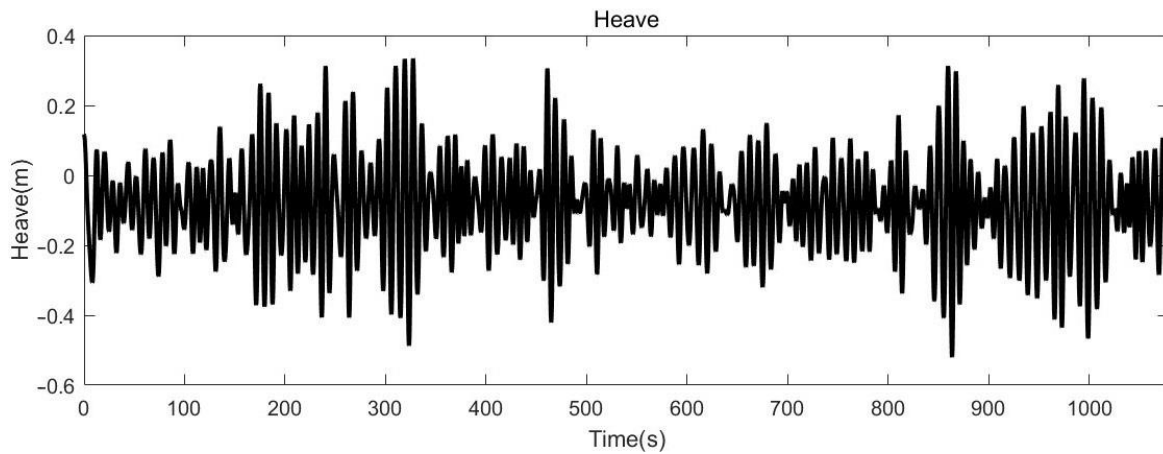


Figure 10. Heave Time Series ( $\bar{\zeta}_W = 2.5 \text{ m}$ ,  $\mu = 15^\circ$ ).

3.2. Pre-Trained Models under Node Conditions

The wave elevation and ship motion series under each node condition are used to train the dual-channel BiLSTM network models. The forecast duration is set to 5 s, 10 s, and 15 s, respectively. Each ship’s motion time series obtained by numerical simulation is divided into a training set and a test set. The samples of the BiLSTM network model training set for each condition node are 5000, the test set is 1000. The training set is used for model training and parameter adjustment, while the test set is utilized to assess the model’s effectiveness. Since the wave elevation probe is located half a ship length ahead of the bow, the forecast time window is set to 15 s, aligning with the time for the wave to propagate to the bow. The dual-channel BiLSTM network structure, depicted in Figure 11, consists of two layers of BiLSTM with 128 and 64 hidden units, respectively. The output layer is a Fully Connected Layer with a dimension of 1, producing the forecast motion response. The loss function adopted is the root mean square error, and the optimizer utilized is Adam. Additionally, to prevent overfitting, DROPOUT is applied to each layer with a parameter set to 0.2.

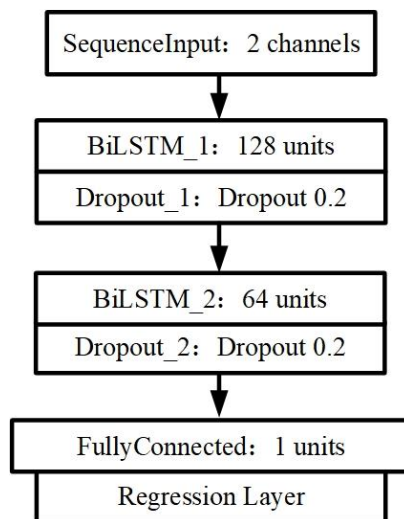


Figure 11. Dual-channel BiLSTM Model Structure.

To evaluate the performance of the neural network model, ship motion forecasts were conducted on the test set of each condition node with forecast durations of 5 s, 10 s, and 15 s. The results were then compared with the actual motion series. To enhance the training efficiency and stability of the model, the Min–Max normalization method was applied to

standardize the data features to the same scale before training. Figures 12 and 13 depict the forecast results after denormalization for some condition node models.

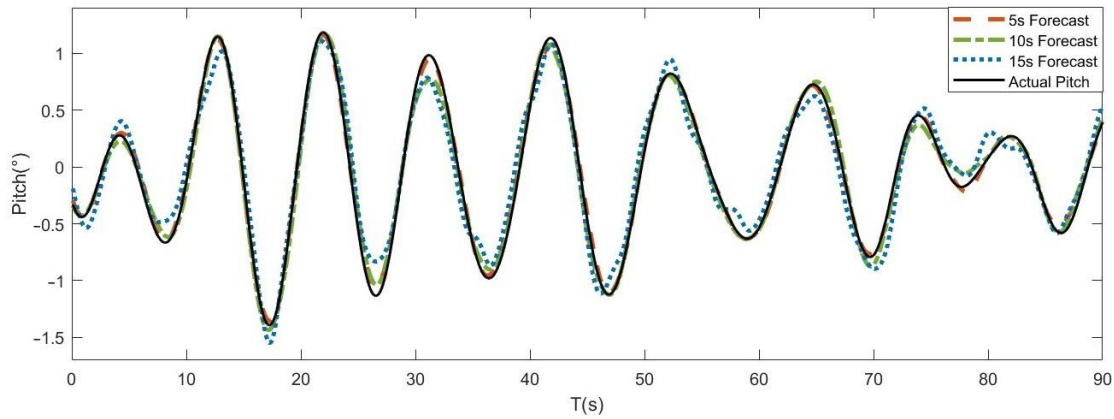


Figure 12. Pitch Forecast Series ( $\bar{\zeta}_W = 4 \text{ m}$ ,  $\mu = 15^\circ$ ).

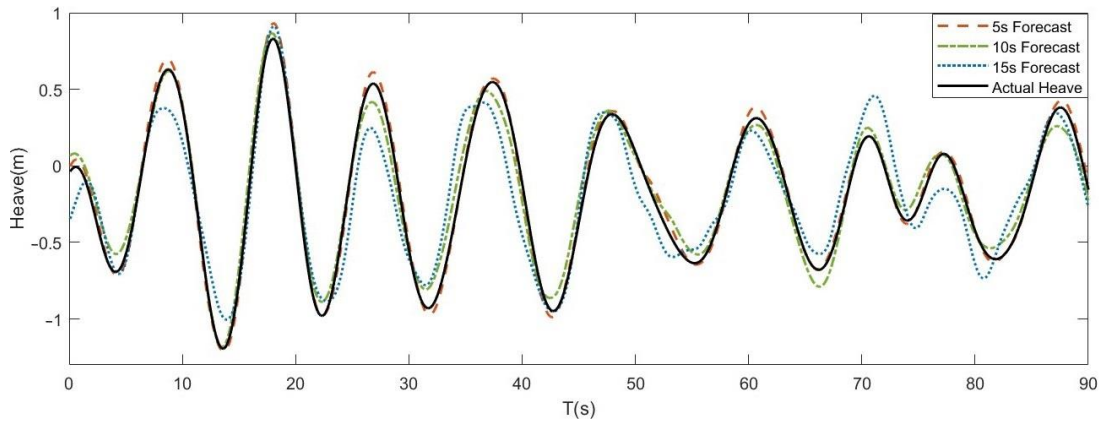


Figure 13. Heave Forecast Series ( $\bar{\zeta}_W = 4 \text{ m}$ ,  $\mu = 15^\circ$ ).

The Mean Absolute Error (*MAE*), Root Mean Square Error (*RMSE*), and Spearman Correlation Coefficient (*R<sub>s</sub>*) were selected to evaluate the forecasting capability of the models. The denormalized test set was used for evaluations. The formulas for the three indicators are as follows:

$$MAE = \frac{1}{n} \sum_{i=1}^n |y_i - \hat{y}_i| \tag{21}$$

$$RMSE = \sqrt{\frac{1}{n} \sum_{i=1}^n (y_i - \hat{y}_i)^2} \tag{22}$$

$$R_s = 1 - \frac{6 \sum_{i=1}^n d_i^2}{n(n^2 - 1)} \tag{23}$$

where,  $y_i$  represents the actual value,  $\hat{y}_i$  is the forecast value, and  $d_i$  is the grade difference between the forecast value and the actual value. *MAE* is the mean absolute value of the observation error, without considering the square of the error. *RMSE* is the square root of the mean square of the forecast errors, assigning greater weight to larger errors. Compared to *MAE*, *RMSE* is more sensitive to large errors. *R<sub>s</sub>* is a rank-based correlation calculation method for assessing the nonlinear relationship between two series. In the context of nonlinear and non-stationary time series, such as ship motion, the Spearman correlation coefficient is robust against outliers and data distribution. Part of the forecast accuracy evaluation results for some pre-trained models are as follows:



### 3.3. Motion Forecast under Non-Node Conditions

By utilizing the pre-trained motion forecast model under node conditions, ship motion under non-node conditions is forecasted. In this section, three different cases are used to evaluate the performance of the model, as illustrated in Table 6.

**Table 6.** Cases Used to Verify the Algorithm.

	Case 1	Case 2	Case 3
$\bar{\zeta}_W$ (Full Scale, m)	1.617	3.235	3.235
$\bar{\zeta}_W$ (Model, m)	0.020	0.040	0.040
$\mu$ (°)	5°	10°	20°

All other things being equal, numerical simulations of the KCS ship model are conducted in Case 1, 2, and 3. The wave elevation at half a ship’s length ahead of the bow and the time series of the ship’s pitch and heave are monitored. The numerical simulation of the full-scale ship motion series length is 135 s. Figures 14–16 illustrate the wave elevation, KCS ship pitch, and heave series in three cases:

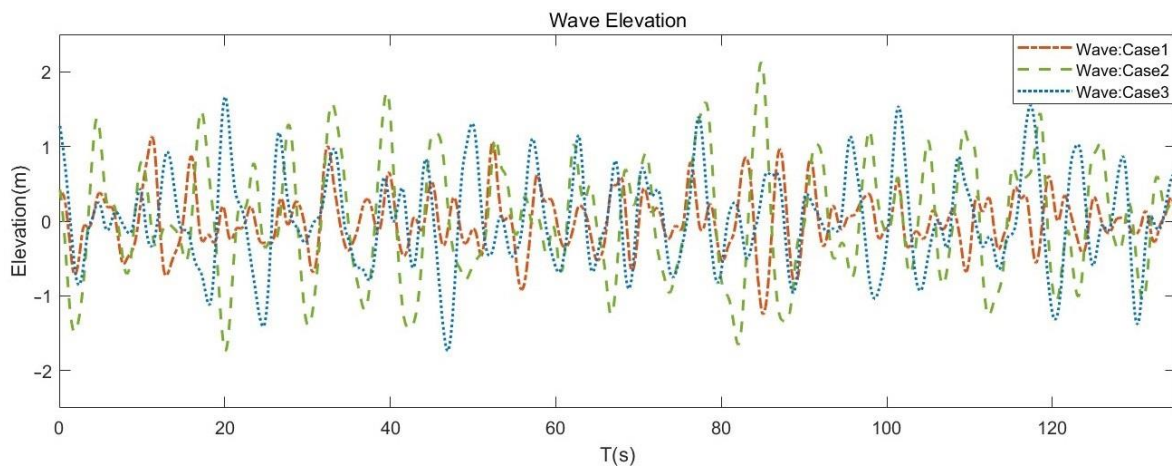


**Figure 14.** Wave Elevation in Three Cases.

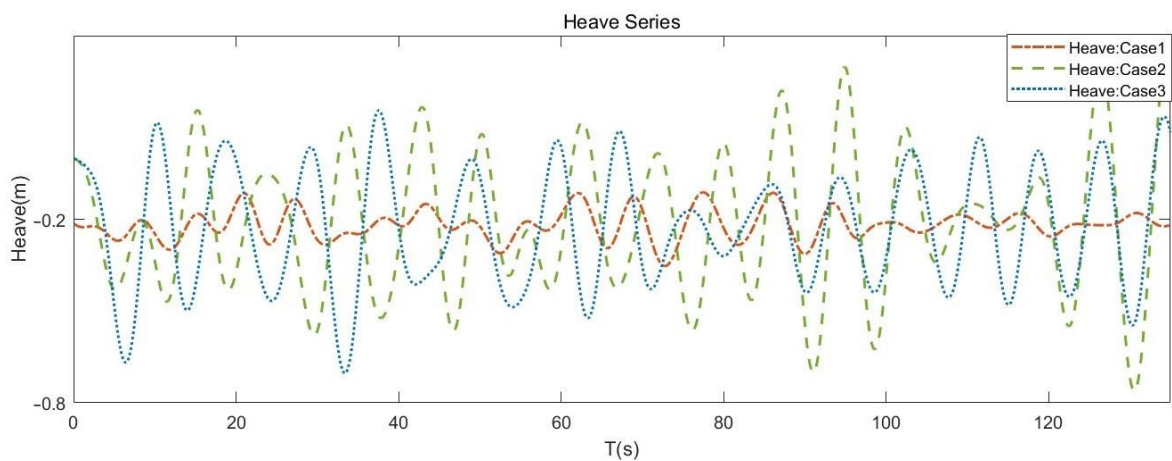


**Figure 15.** Heave Series in Three Cases.

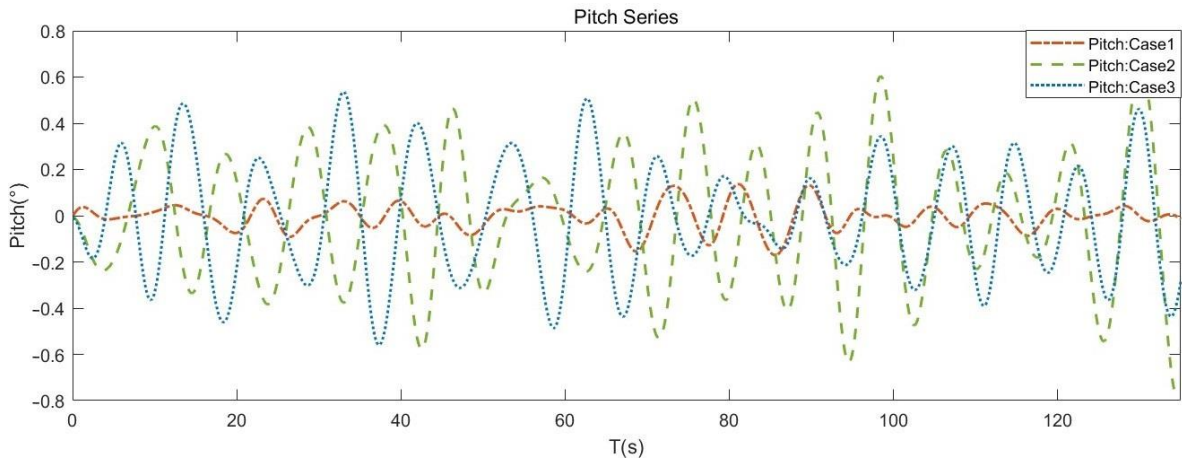


Figure 16. Pitch Series in Three Cases.

Ship motion series in three cases are forecasted by the method. Pre-trained node models are selected based on the correlation between node conditions and current conditions. The pre-trained model size is shown in Table 7 and selection for the three cases is depicted in Figures 17–19:

Table 7. Model Size.

	First-Order	First-Order	First-Order	First-Order
Params (K)	298.6	597.2	895.8	1194.5

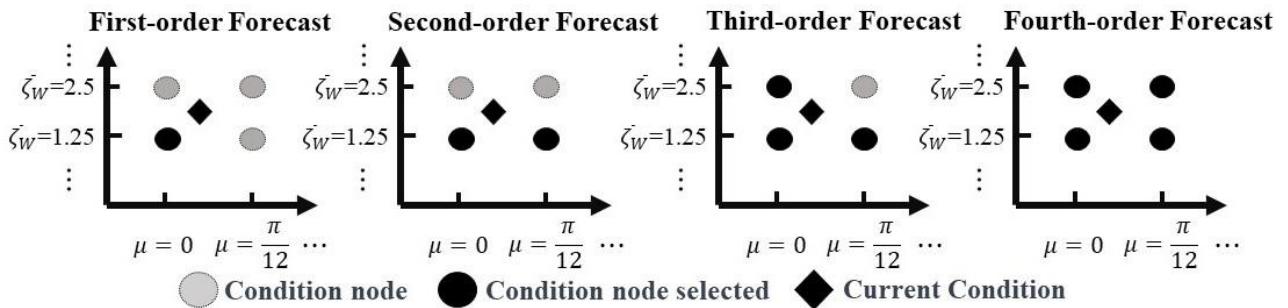


Figure 17. Pre-trained Model Selection in Case 1.

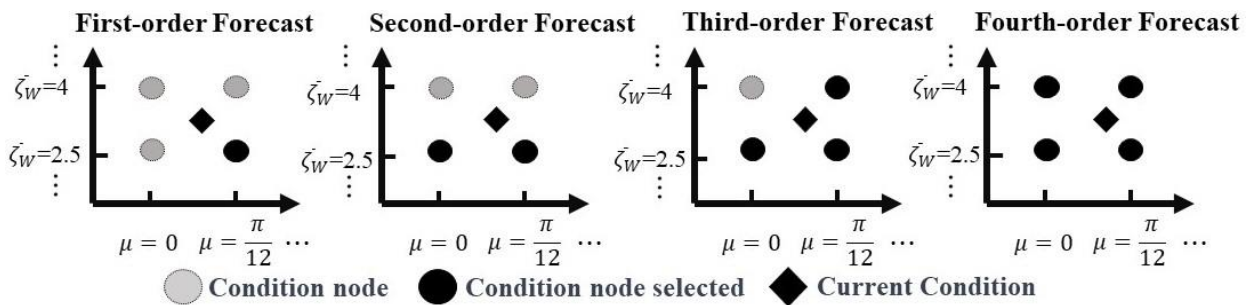


Figure 18. Pre-trained Model Selection in Case 2.

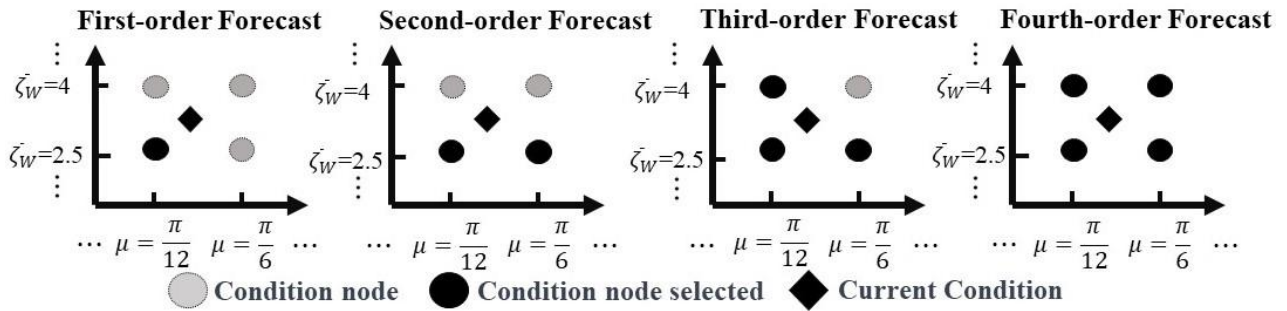


Figure 19. Pre-trained Model Selection in Case 3.

Pitch and heave motion forecasts with a duration of 5 s, 10 s, and 15 s are conducted for three cases, respectively. Leveraging the pre-training model selection results, 1-4 order models are used for each motion forecast. Throughout this experiment, the regression coefficients of the multi-order forecast model were set to be calculated and updated every 20 s. The forecast pitch series for case 3 is shown in Figures 20–22.

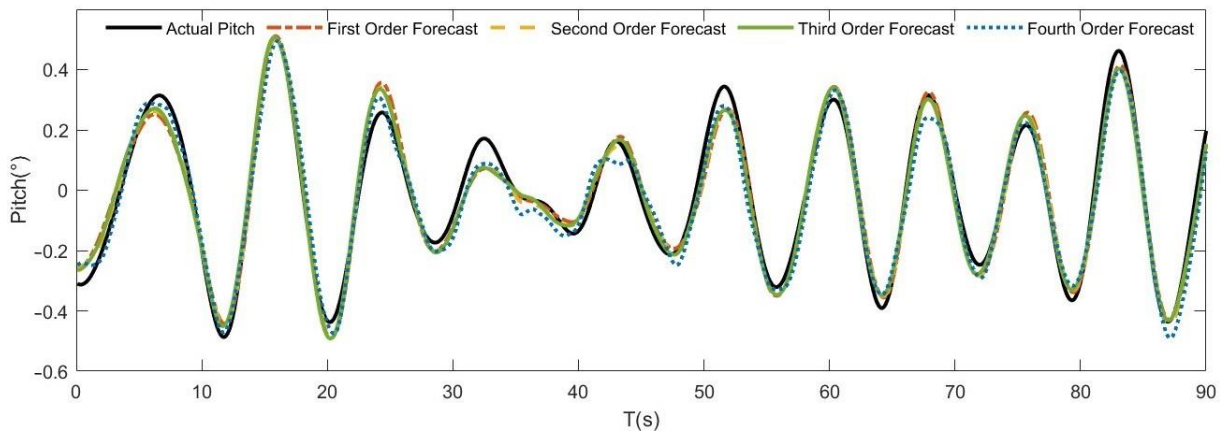


Figure 20. 1st–4th Pitch Forecast of 5s Duration in Case 3.

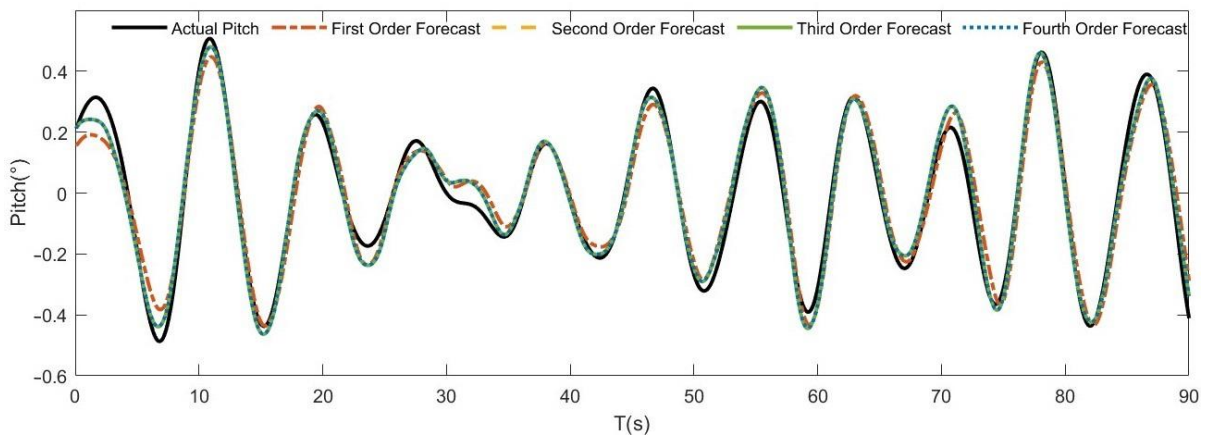


Figure 21. 1st–4th Pitch Forecast in 10s Duration in Case 3.

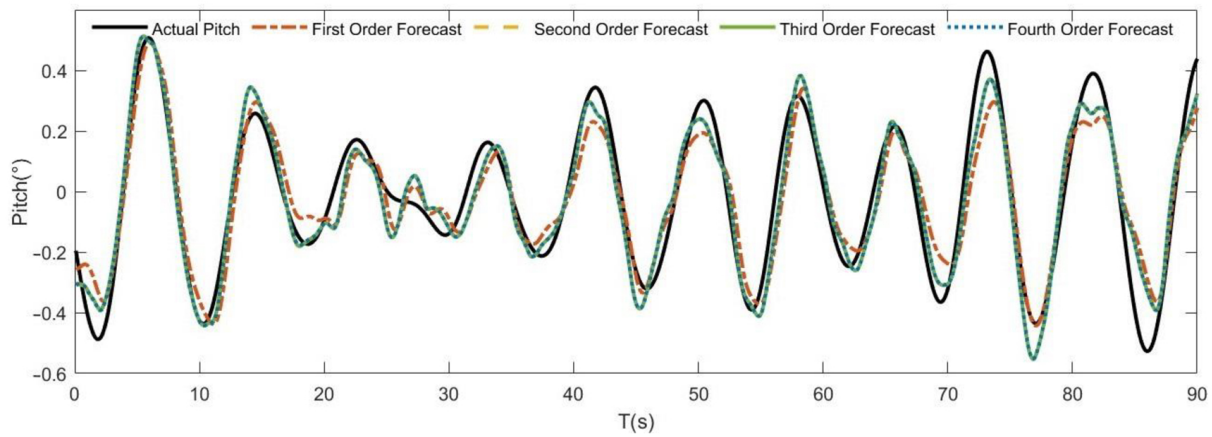


Figure 22. 1st–4th Pitch Forecast in 15s Duration in Case 3.

MAE, RMSE, and  $R_s$  are used to evaluate the forecast accuracy. The forecast results of three cases are presented in Tables 8–11. The results reveal that the forecast accuracy of the multi-order model is higher than that of the first-order model. The first-order forecast model exhibits the largest forecast error and the least accuracy under identical conditions and forecast durations. However, since the first-order forecasted model is essentially a dynamic model selection in the absence of optimal computation, it has the smallest number of parameters and the fastest forecast speed.

Table 8. First-order Model Forecast.

		Case 1		Case 2		Case 3	
		Pitch	Heave	Pitch	Heave	Pitch	Heave
5 s Forecast	MAE	0.0118	0.0109	0.0462	0.0495	0.0360	0.0267
	RMSE	0.0291	0.0188	0.0583	0.0627	0.0437	0.0523
	$R_s$	0.9594	0.9531	0.9801	0.9736	0.9821	0.9750
10 s Forecast	MAE	0.0207	0.0282	0.0542	0.0493	0.0402	0.0415
	RMSE	0.0314	0.0340	0.0643	0.0644	0.0478	0.0548
	$R_s$	0.9415	0.9495	0.9764	0.9698	0.9807	0.9522
15 s Forecast	MAE	0.0387	0.0305	0.0935	0.0753	0.0701	0.0618
	RMSE	0.0442	0.0479	0.1163	0.0959	0.0892	0.0784
	$R_s$	0.9139	0.9277	0.9410	0.9105	0.9384	0.9132

Table 9. Second-order Model Forecast.

		Case 1		Case 2		Case 3	
		Pitch	Heave	Pitch	Heave	Pitch	Heave
5 s Forecast	MAE	0.0102	0.0103	0.0443	0.0455	0.0349	0.0226
	RMSE	0.0265	0.0164	0.0563	0.0572	0.0410	0.0338
	$R_s$	0.9643	0.9562	0.9814	0.9749	0.9847	0.9826
10 s Forecast	MAE	0.0193	0.0257	0.0465	0.0468	0.0302	0.0397
	RMSE	0.0302	0.0339	0.0590	0.0600	0.0368	0.0540
	$R_s$	0.9430	0.9546	0.9790	0.9698	0.9879	0.9545
15 s Forecast	MAE	0.0346	0.0287	0.0628	0.0654	0.0677	0.0592
	RMSE	0.0412	0.0455	0.0788	0.0838	0.0833	0.0745
	$R_s$	0.9315	0.9410	0.9607	0.9233	0.9534	0.9237

**Table 10.** Third-order Model Forecast.

		Case 1		Case 2		Case 3	
		Pitch	Heave	Pitch	Heave	Pitch	Heave
5 s Forecast	MAE	0.0101	0.0103	0.0442	0.0455	0.0319	0.0220
	RMSE	0.0265	0.0164	0.0564	0.0572	0.0391	0.0328
	$R_s$	0.9644	0.9562	0.9814	0.9741	0.9859	0.9833
10 s Forecast	MAE	0.0193	0.0258	0.0465	0.0467	0.0302	0.0390
	RMSE	0.0301	0.0339	0.0590	0.0598	0.0368	0.0540
	$R_s$	0.9430	0.9546	0.9790	0.9698	0.9879	0.9546
15 s Forecast	MAE	0.0344	0.0295	0.0627	0.0643	0.0677	0.0592
	RMSE	0.0412	0.0451	0.0787	0.0832	0.0833	0.0745
	$R_s$	0.9317	0.9413	0.9607	0.9254	0.9534	0.9237

**Table 11.** Fourth-order Model Forecast.

		Case 1		Case 2		Case 3	
		Pitch	Heave	Pitch	Heave	Pitch	Heave
5 s Forecast	MAE	0.0102	0.0103	0.0442	0.0455	0.0319	0.0220
	RMSE	0.0265	0.0166	0.0563	0.0572	0.0391	0.0328
	$R_s$	0.9643	0.9562	0.9814	0.9741	0.9858	0.9833
10 s Forecast	MAE	0.0193	0.0257	0.0465	0.0467	0.0301	0.0397
	RMSE	0.0302	0.0339	0.0590	0.0598	0.0368	0.0539
	$R_s$	0.9430	0.9545	0.9790	0.9698	0.9879	0.9545
15 s Forecast	MAE	0.0344	0.0295	0.0628	0.0643	0.0679	0.0592
	RMSE	0.0412	0.0455	0.0788	0.0832	0.0836	0.0745
	$R_s$	0.9315	0.9410	0.9607	0.9254	0.9531	0.9237

When the multi-order model is used for forecasting, both *MAE* and *RMSE* exhibit a 4% to 15% decrease compared with the first-order model forecast in all forecast durations. In the 5s duration forecast,  $R_s$  of the second-order forecast model experiences an approximately 0.5% increase. This is because the forecast duration is relatively short, so the distinctiveness of series characteristics is not obvious. In the 10s duration forecast,  $R_s$  of the second-order model forecast increases by 0.5% to 1%. In the 15 s duration forecast, the  $R_s$  increases by about 2%. This is because as the forecast duration increases, the distinctiveness of the series distribution characteristics becomes more significant. Therefore, the improvement of  $R_s$  in forecasting is also greater in second-order model. In the multi-order model prediction, the *MAE* and *RMSE* of the third-order forecast model are reduced by less than 5% compared with the second-order model, with a slight or no improvement in  $R_s$ . Compared with the third-order prediction model, the fourth-order forecast model exhibits nearly no improvement across the three evaluation indicators while having the largest number of parameters.

In conclusion, for ship motion forecasting with a 5-s forecasting duration, the first-order forecast model demonstrates a quicker response and a smaller model size, making it more suitable for very short-term forecast tasks with high real-time requirements and limited resources [33]. The second-order forecast model showcases higher accuracy and smaller errors. As the forecast duration increases to 10 s and 15 s, the accuracy of the second-order model improves even more significantly. Although the accuracy of the third-order model is slightly higher than that of the second-order model, the size of the model and computation time are also higher. In comparison, the fourth-order model demonstrates almost no improvement in accuracy, and it has the largest model size. The selection of different forecast models necessitates trade-offs between forecast performance, computational efficiency, and model size.

#### 4. Conclusions

While conducting operations at the actual sea surface, ships frequently encounter diverse sea conditions, such as waves, tidal currents, and wind forces. A data-driven ship motion forecast method is proposed in this paper, aiming at the problem of single application scenarios and the diminished generalization ability of existing methods in ship motion forecasting. This model integrates machine learning techniques with potential flow theory methods to enhance forecasting accuracy and broaden its applicability. The main components are as follows:

(1) Substantial numerical simulations using the KCS ship model are conducted. The obtained motion response series were then used to train BiLSTM network models, creating a pre-trained forecast model database with varying forecast durations.

(2) A calculation method of condition correlation is proposed, facilitating the 1–4 order forecast models, which are determined through the method. The Golden Jackal optimization algorithm is employed to compute the regression coefficients for each pre-trained model. The dynamic model averaging is calculated to forecast the motion of the ship under non-node conditions.

The results indicate that when forecasting ship motion under non-node conditions, the first-order forecast model exhibits the lowest accuracy compared with the multi-order model. As the forecast duration extends, the accuracy of the multi-order forecast model shows more obvious improvement. While the third-order forecast model demonstrates slightly superior performance to the second-order model, it comes at the cost of a larger number of model parameters. The fourth-order prediction model has the largest number of parameters and almost no improvement in accuracy.

The approach in this study makes forecasting more comprehensive and reliable, considering the diversity of sea conditions and ship motion states. The pre-training model can be better adapted to the ship motion forecast under non-node conditions by making full use of the data under node conditions. The method is of significance for improving safety and operational efficiency in offshore operations. However, challenges persist in ship motion and wave elevation detection. The accuracy of a ship motion forecast can be affected by the presence of missing data and noise. Further enhancements are needed in the robustness of the forecast model to address these concerns. In subsequent research, the accurate identification of wave elevations on the sea surface and the model's adaptability to ship motion under high sea conditions will also be studied. Additional research methods, such as Variational Mode Decomposition, may be explored to augment the algorithm's capacity for forecasting ship motion in challenging sea conditions.

**Author Contributions:** Conceptualization, W.L.; Data curation, Y.M.; Formal analysis, Y.M.; Methodology, Z.J.; Project administration, W.L.; Resources, Z.J.; Supervision, W.L.; Validation, Y.M.; Writing—original draft, Z.J.; Writing—review and editing, Z.J. and W.L. All authors have read and agreed to the published version of the manuscript.

**Funding:** This research received no external funding.

**Institutional Review Board Statement:** Not applicable.

**Informed Consent Statement:** Not applicable.

**Data Availability Statement:** Data will be made available on request.

**Conflicts of Interest:** The research was conducted in the absence of any commercial or financial relationships that could be construed as a potential conflict of interest.

#### References

1. Kubo, M.; Mizui, S.; Inoue, K. Safety evaluation of ship entering a harbor under severe wave conditions. In Proceedings of the 10th International Offshore and Polar Engineering Conference (ISOPE-2000), Seattle, WA, USA, 28 May–2 June 2000; Grundy, P., Koo, J., Langen, I., Knapp, R., Eds.; ISOPE: Mountain View, CA, USA, 2000; Volume IV, pp. 330–336.
2. Chu, Y.G.; Li, G.Y.; Hatledal, L.I.; Holmeset, F.T.; Zhang, H.X. Coupling of dynamic reaction forces of a heavy load crane and ship motion responses in waves. *Ships Offshore Struct.* **2021**, *16*, 58–67. [[CrossRef](#)]

3. Neupert, J.; Mahl, T.; Haessig, B.; Sawodny, O.; Schneider, K. A heave compensation approach for offshore cranes. In Proceedings of the 2008 American Control Conference, Seattle, WA, USA, 11–13 June 2008; IEEE: Piscataway, NJ, USA, 2008; Volume 1–12, p. 538.
4. Yang, H.; Pan, Z.; Bai, W. Review of Time Series Prediction Methods. *Comput. Sci.* **2019**, *46*, 21–28.
5. Nie, Z.H.; Lu, Z.F.; Lai, P.; Zhou, J.P.; Yao, F.J. Short-term Prediction of Large Ship Motion Based on Empirical Mode Decomposition and Autoregressive Model. In Proceedings of the 2022 IEEE 6th Advanced Information Technology, Electronic and Automation Control Conference (IAEAC), Beijing, China, 3–5 October 2022; IEEE: Piscataway, NJ, USA, 2022; pp. 933–937.
6. Peng, X.Y.; Zhang, B.; Rong, L.H. A robust unscented Kalman filter and its application in estimating dynamic positioning ship motion states. *J. Mar. Sci. Technol.* **2019**, *24*, 1265–1279. [[CrossRef](#)]
7. Jiang, H.; Duan, S.L.; Huang, L.M.; Han, Y.; Yang, H.; Ma, Q.W. Scale effects in AR model real-time ship motion prediction. *Ocean Eng.* **2020**, *203*, 107202. [[CrossRef](#)]
8. Takami, T.; Nielsen, U.D.; Jensen, J.J. Real-time deterministic prediction of wave-induced ship responses based on short-time measurements. *Ocean Eng.* **2021**, *221*, 108503. [[CrossRef](#)]
9. Ramadevi, B.; Bingi, K. Chaotic Time Series Forecasting Approaches Using Machine Learning Techniques: A Review. *Symmetry* **2022**, *14*, 955. [[CrossRef](#)]
10. D’Agostino, D.; Serani, A.; Stern, F.; Diez, M. Time-series forecasting for ships maneuvering in waves via recurrent-type neural networks. *J. Ocean Eng. Mar. Energy* **2022**, *8*, 479–487. [[CrossRef](#)]
11. Silva, K.M.; Maki, K.J. Data-Driven system identification of 6-DoF ship motion in waves with neural networks. *Appl. Ocean Res.* **2022**, *125*, 103222. [[CrossRef](#)]
12. Diez, M.; Serani, A.; Campana, E.F.; Stern, F. Time-series forecasting of ships maneuvering in waves via dynamic mode decomposition. *J. Ocean Eng. Mar. Energy* **2022**, *8*, 471–478. [[CrossRef](#)]
13. Burkart, N.; Huber, M.F. A Survey on the Explainability of Supervised Machine Learning. *J. Artif. Intell. Res.* **2021**, *70*, 245–317. [[CrossRef](#)]
14. Suhermi, N.; Suhartono; Prastyo, D.D.; Ali, B. Roll motion prediction using a hybrid deep learning and ARIMA model. In Proceedings of the 3rd INNS Conference on Big Data and Deep Learning (INNS BDDL), Kota Denpasar, Indonesia, 17–19 April 2018; Ozawa, S., Tan, A.H., Angelov, P.P., Roy, A., Pratama, M., Eds.; Elsevier: Amsterdam, The Netherlands, 2018; Volume 144, pp. 251–258.
15. Xu, W.Z.; Maki, K.J.; Silva, K.M. A data-driven model for nonlinear marine dynamics. *Ocean Eng.* **2021**, *236*, 109469. [[CrossRef](#)]
16. Ye, R.; Dai, Q. A novel transfer learning framework for time series forecasting. *Knowl.-Based Syst.* **2018**, *156*, 74–99. [[CrossRef](#)]
17. Du, Y.T.; Wang, J.D.; Feng, W.J.; Pan, S.N.; Qin, T.; Xu, R.J.; Wang, C.J. AdaRNN: Adaptive Learning and Forecasting for Time Series. In Proceedings of the 30th ACM International Conference on Information & Knowledge Management (CIKM), Gold Coast, Australia, 1–5 November 2021; ACM: New York, NY, USA, 2021; pp. 402–411.
18. Dormann, C.F.; Calabrese, J.M.; Guillera-Arroita, G.; Matechou, E.; Bahn, V.; Barton, K.; Beale, C.M.; Ciuti, S.; Elith, J.; Gerstner, K.; et al. Model averaging in ecology: A review of Bayesian, information-theoretic, and tactical approaches for predictive inference. *Ecol. Monogr.* **2018**, *88*, 485–504. [[CrossRef](#)]
19. Darbandsari, P.; Coulibaly, P. Introducing entropy-based Bayesian model averaging for streamflow forecast. *J. Hydrol.* **2020**, *591*, 125577. [[CrossRef](#)]
20. Naser, H. Estimating and forecasting the real prices of crude oil: A data rich model using a dynamic model averaging (DMA) approach. *Energy Econ.* **2016**, *56*, 75–87. [[CrossRef](#)]
21. Jiang, Y.S.; Jia, M.Q.; Zhang, B.; Deng, L.W. Ship Attitude Prediction Model Based on Cross-Parallel Algorithm Optimized Neural Network. *IEEE Access* **2022**, *10*, 77857–77871. [[CrossRef](#)]
22. Wei, Y.Y.; Chen, Z.Z.; Zhao, C.; Tu, Y.H.; Chen, X.; Yang, R. A BiLSTM hybrid model for ship roll multi-step forecasting based on decomposition and hyperparameter optimization. *Ocean Eng.* **2021**, *242*, 110138. [[CrossRef](#)]
23. Zhang, G.Y.; Tan, F.; Wu, Y.X. Ship Motion Attitude Prediction Based on an Adaptive Dynamic Particle Swarm Optimization Algorithm and Bidirectional LSTM Neural Network. *IEEE Access* **2020**, *8*, 90087–90098. [[CrossRef](#)]
24. Do, K.D.; Jiang, Z.P.; Pan, J. Robust global stabilization of underactuated ships on a linear course: State and output feedback. *Int. J. Control* **2003**, *76*, 1–17. [[CrossRef](#)]
25. Seo, M.G.; Kim, Y. Numerical analysis on ship maneuvering coupled with ship motion in waves. *Ocean Eng.* **2011**, *38*, 1934–1945. [[CrossRef](#)]
26. Yang, W.; Liang, Y.K.; Leng, J.X.; Li, M. The Autocorrelation Function Obtained from the Pierson-Moskowitz Spectrum. In Proceedings of the Global Oceans 2020: Singapore—U.S. Gulf Coast, Biloxi, MS, USA, 5–30 October 2020; IEEE: Piscataway, NJ, USA, 2020.
27. Peng, T.; Zhang, C.; Zhou, J.Z.; Nazir, M.S. An integrated framework of Bi-directional long-short term memory (BiLSTM) based on sine cosine algorithm for hourly solar radiation forecasting. *Energy* **2021**, *221*, 119887. [[CrossRef](#)]
28. Yu, Y.; Si, X.S.; Hu, C.H.; Zhang, J.X. A Review of Recurrent Neural Networks: LSTM Cells and Network Architectures. *Neural Comput.* **2019**, *31*, 1235–1270. [[CrossRef](#)]
29. Raftery, A.E.; Kárny, M.; Ettler, P. Online Prediction Under Model Uncertainty via Dynamic Model Averaging: Application to a Cold Rolling Mill. *Technometrics* **2010**, *52*, 52–66. [[CrossRef](#)]

30. Chopra, N.; Ansari, M.M. Golden jackal optimization: A novel nature-inspired optimizer for engineering applications. *Expert Syst. Appl.* **2022**, *198*, 116924. [[CrossRef](#)]
31. GB/T 42176-2022; The Grade of Wave Height. General Administration of Quality Supervision. Inspection and Quarantine of the People's Republic of China: Beijing, China, 2022.
32. Shen, Z.; Wan, D.; Carrica, P.M. Dynamic overset grids in OpenFOAM with application to KCS self-propulsion and maneuvering. *Ocean Eng.* **2015**, *108*, 287–306. [[CrossRef](#)]
33. Li, Y.; Xiao, L.; Wei, H.; Kou, Y.; Li, X. Comparative Study of Two Neural Network Models for Online Prediction of Wave Run-up on Semi-Submersible. *Shipbuild. China* **2023**, *64*, 28–40.

**Disclaimer/Publisher's Note:** The statements, opinions and data contained in all publications are solely those of the individual author(s) and contributor(s) and not of MDPI and/or the editor(s). MDPI and/or the editor(s) disclaim responsibility for any injury to people or property resulting from any ideas, methods, instructions or products referred to in the content.